Supporting Information

Controllable Structure Reconstruction of Nickel-Iron Compounds toward Highly Efficient Oxygen Evolution

Azhar Mahmood†, Qiangmin Yu†, Yuting Luo, Zhiyuan Zhang, Chi Zhang, Ling Qiu and Bilu Liu*

Shenzhen Geim Graphene Center (SGC), Tsinghua-Berkeley Shenzhen Institute (TBSI) and Tsinghua Shenzhen International Graduate School (TSIGS), Tsinghua University, Shenzhen 518055, PR China.

Author contributions

†A.M. and Q.Y. contributed equally to this work.

Corresponding author

Bilu Liu. Email: bilu.liu@sz.tsinghua.edu,cn

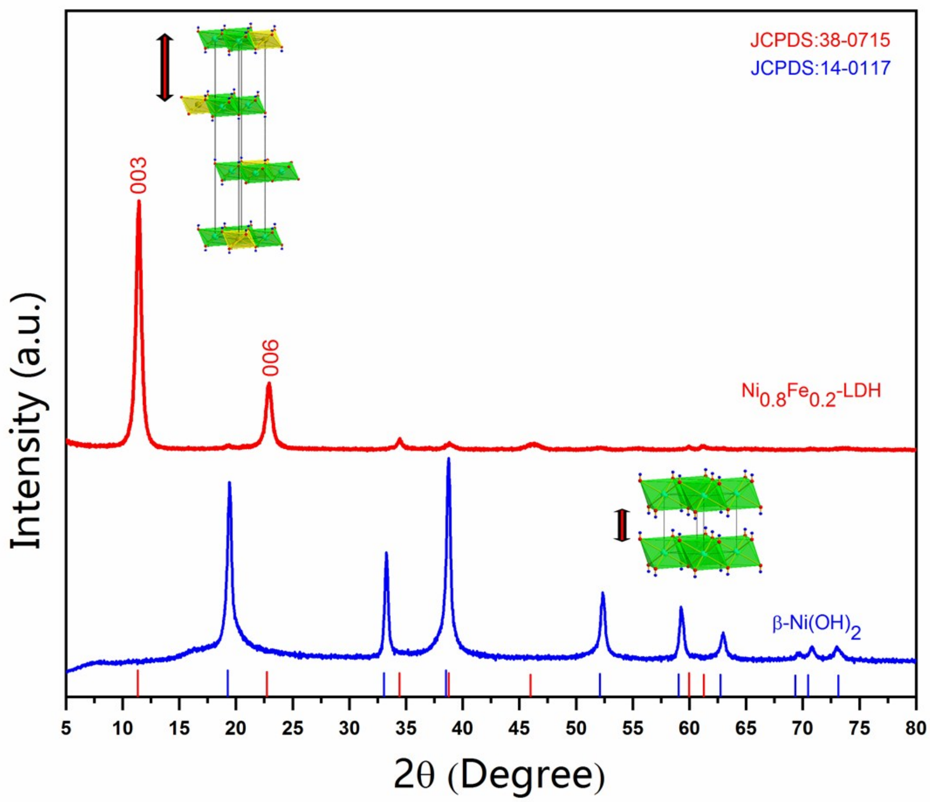

Figure S1. XRD patterns and schematic crystal structures of β-$Ni(OH)_2$ and $Ni_{0.8}Fe_{0.2}$-LDH. The broad diffraction peaks at 11.22° and 23.7°, corresponding to the (003) and (006) lattice planes associated with the interlayer spacing of the $Ni_{0.8}Fe_{0.2}$-LDH.[1] The peak positions and sharpness of the reflections confirm the formation of LDH phase with large interlayer space compared to that of β-$Ni(OH)_2$.

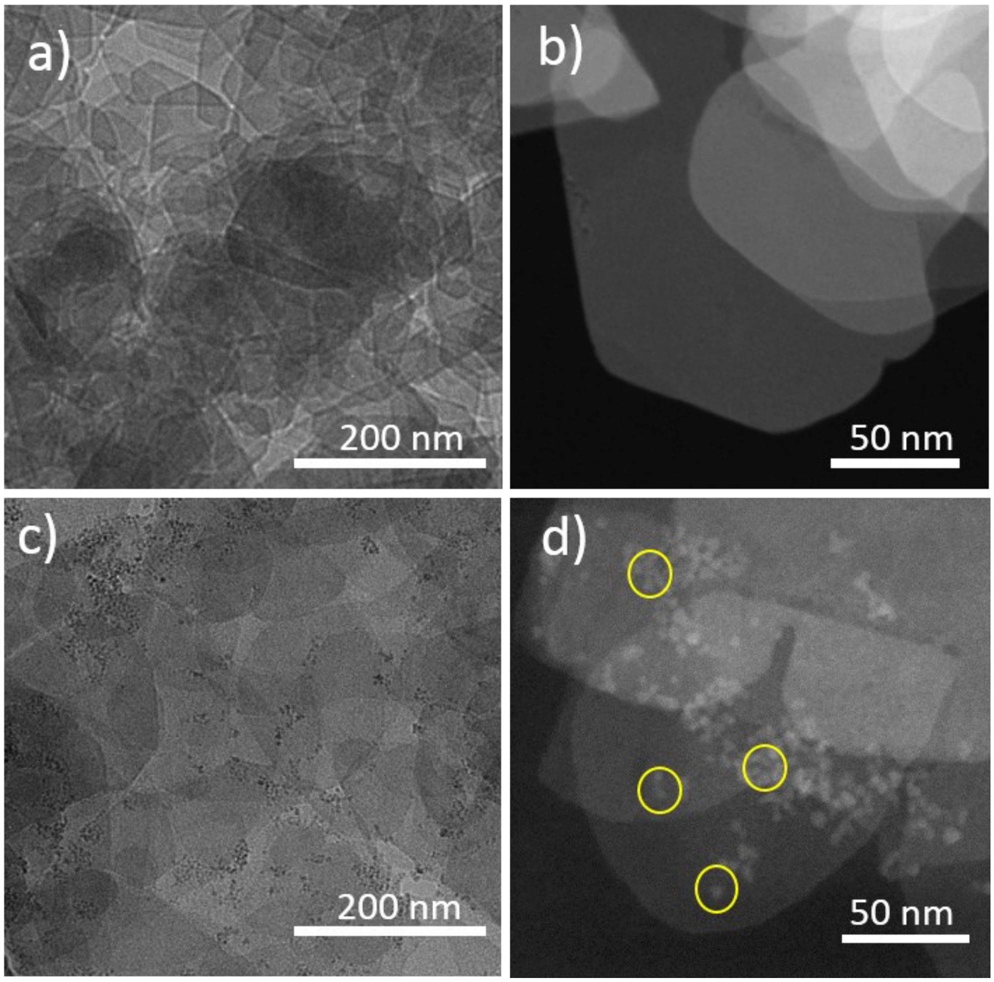

Figure S2. a) TEM, (b) HAADF-STEM of $Ni_{0.8}Fe_{0.2}$-LDH with lower ratio of Fe. (c) TEM, (d) HAADF-STEM of $Ni_{0.7}Fe_{0.3}$-LDH with higher ratio of Fe. HAADF-STEM images clearly show that slight increase of Fe-precursor, causes iron redundant phase nanoparticles.

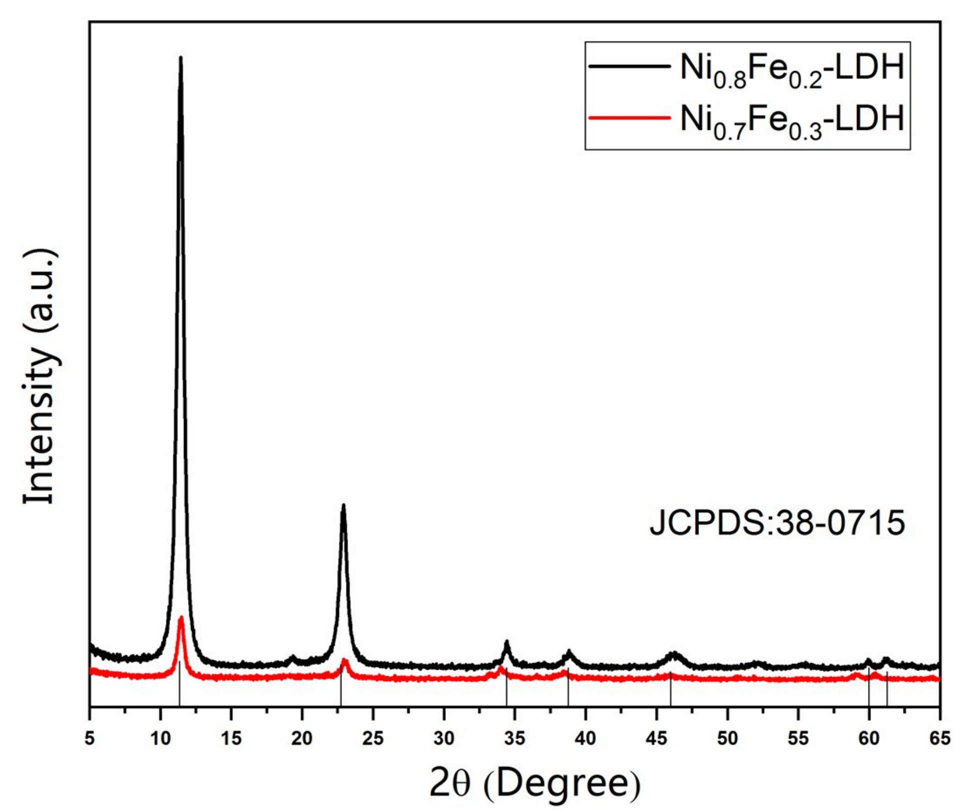

Figure S3. Comparison of XRD patterns of $Ni_{0.8}Fe_{0.2}$-LDH and $Ni_{0.7}Fe_{0.3}$-LDH synthesized under the similar experimental conditions with slight difference of iron precursor. Pattern of $Ni_{0.7}Fe_{0.3}$-LDH clearly showing that, slight enhancement of Fe has no obvious effect on the crystal structure of LDH.

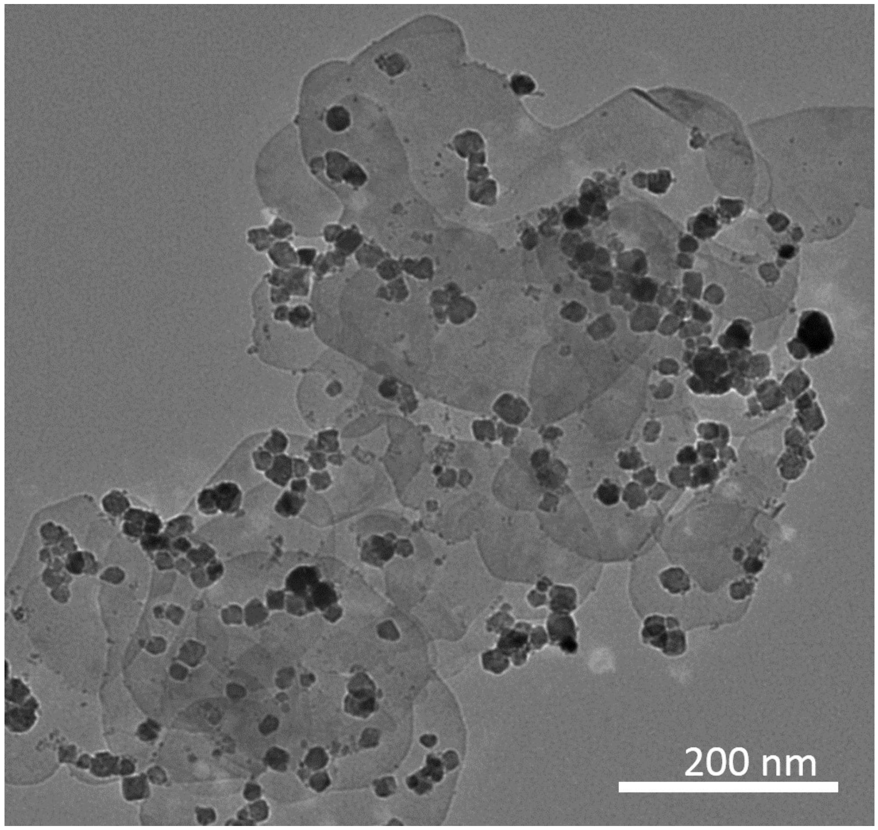

Figure S4. TEM image of the $Ni_{0.5}Fe_{0.5}$-LDH with equal ratio of Ni and Fe precursors collected at 150 °C after 48 h. TEM image of $Ni_{0.5}Fe_{0.5}$-LDH showing that at equal ratio of precursors $NiFe_2O_4$ nanograins appears on the entire surface of $Ni_{0.5}Fe_{0.5}$-LDH nanosheets. These $NiFe_2O_4$ nanoparticles may block the active sites of NiFe-LDH phase and leads to the low OER activity.

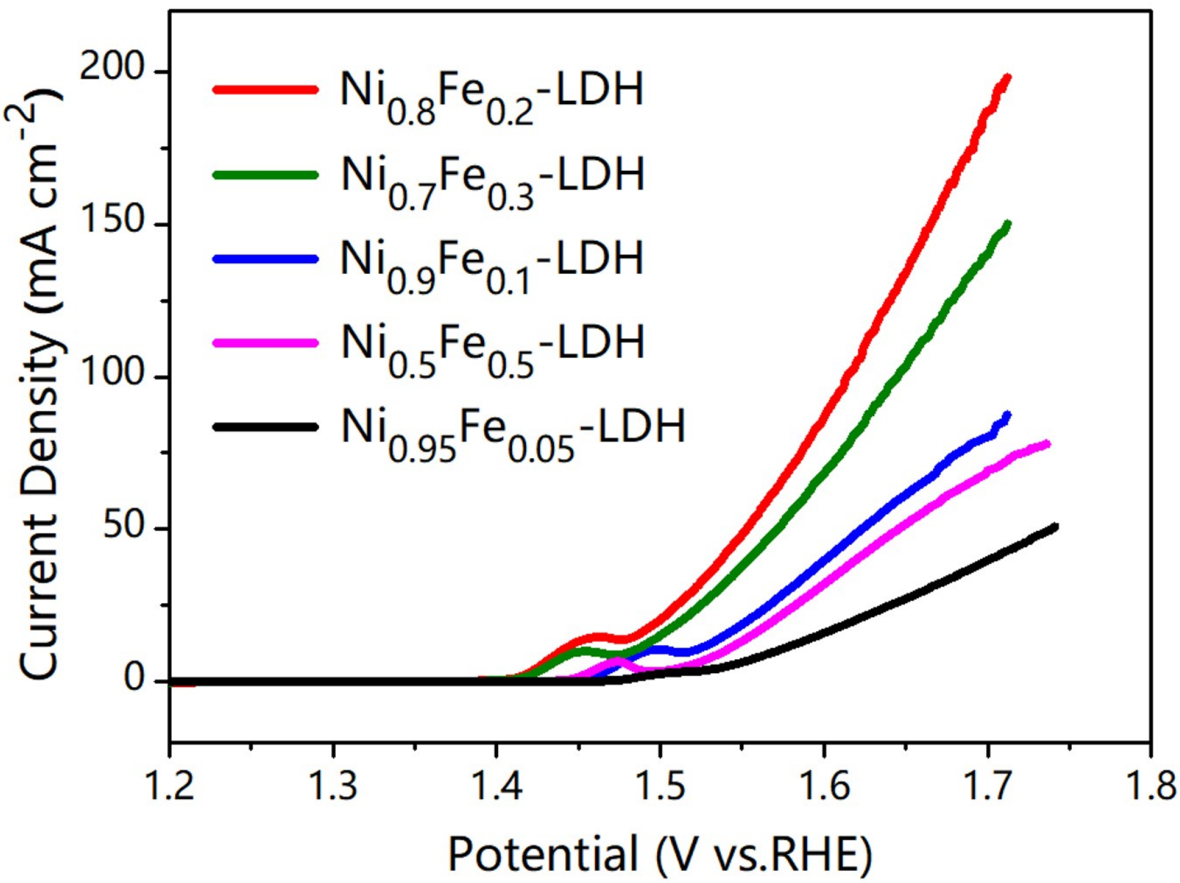

Figure S5. OER polarization curves of NiFe-LDH catalysts with different Fe contents.

The linear sweep voltammograms of NiFe-LDH catalysts synthesized with different molar ratio of precursors showing that OER performance of $Ni_{0.95}Fe_{0.05}$-LDH, $Ni_{0.9}Fe_{0.1}$-LDH and $Ni_{0.8}Fe_{0.2}$-LDH gradually increases with the increase of Fe content. While, OER activity of $Ni_{0.7}Fe_{0.3}$-LDH and $Ni_{0.5}Fe_{0.5}$-LDH decreases with further increase of Fe contents. This decrease in OER performance is due to the formation of redundant phases of FeO_x on the surface of LDH, which are electrochemically inert for the OER and hinder the exposure of the active sites on the surface of LDH nanosheets.

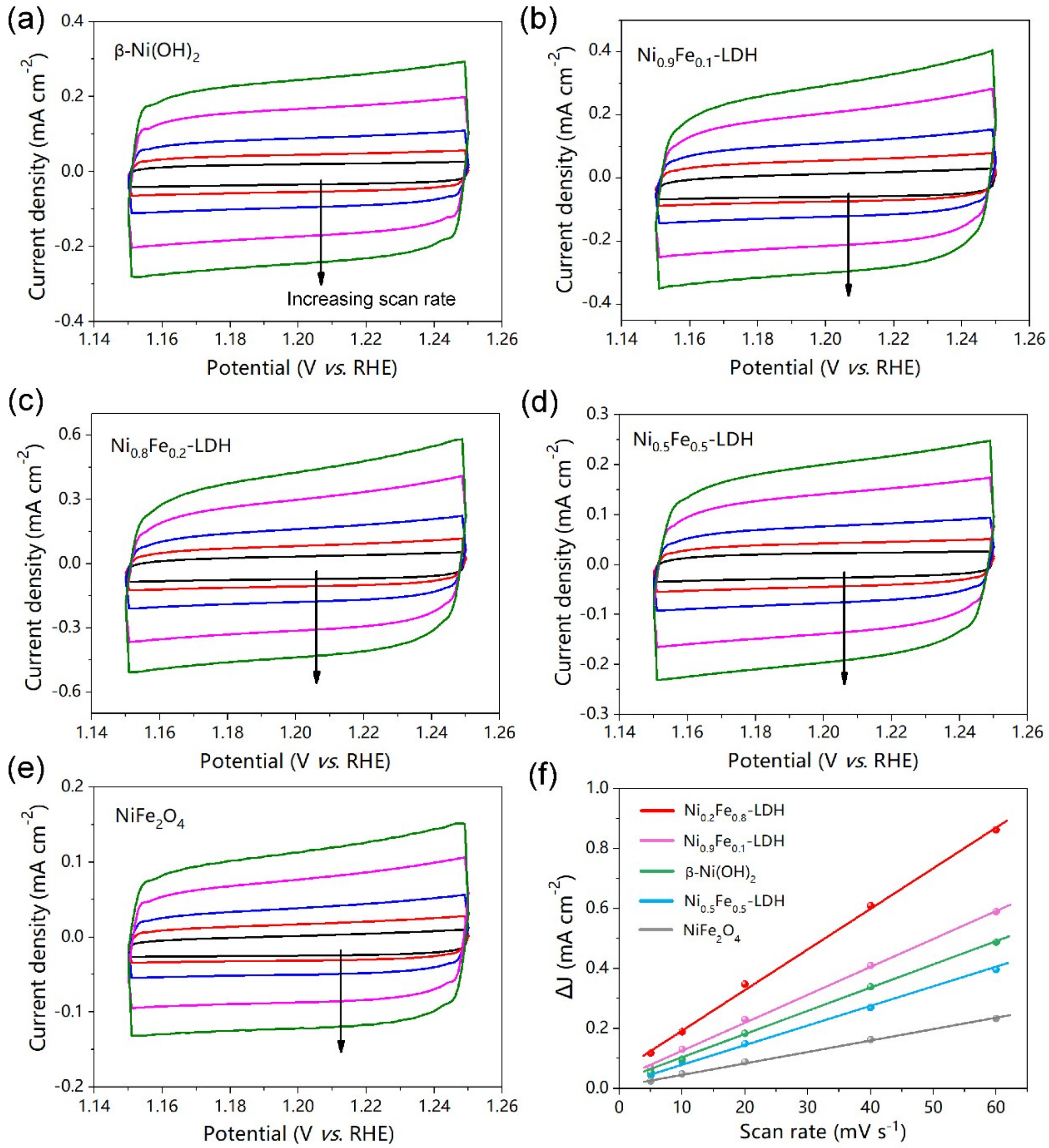

Figure S6. CV scans of different samples measured at a non-Faradaic region range from 1.15 to 1.25 V, with various potential scan rates (5-60 mV s^{-1}). (a) *β*-$Ni(OH)_2$. (b) $Ni_{0.9}Fe_{0.1}$-LDH. (c) $Ni_{0.8}Fe_{0.2}$-LDH. (d) $Ni_{0.5}Fe_{0.5}$-LDH. (e) $NiFe_2O_4$. (f) A capacitive currents (J_a-J_c) at 1.2 V against the scan rate, where the slope of the fitted line was used to calculate the electrochemical double layer capacitance (C_{dl}).

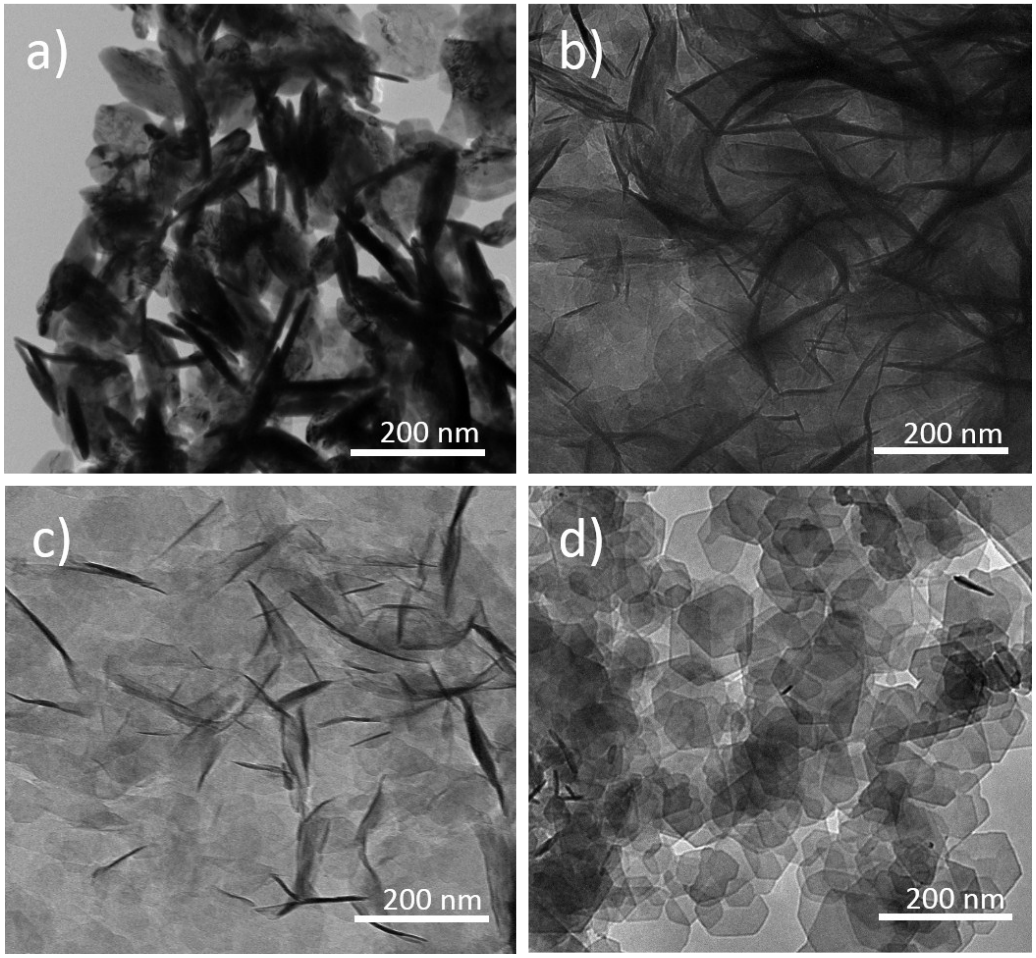

Figure S7. TEM images of the (a) β-Ni(OH)$_2$, (b) $Ni_{0.95}Fe_{0.05}$-LDH, (c) $Ni_{0.9}Fe_{0.1}$-LDH and (d) $Ni_{0.8}Fe_{0.2}$-LDH collected at 150 °C after 48 h. TEM images shows that aggregated shape changes into well-defined hexagonal shape after the doping of iron.

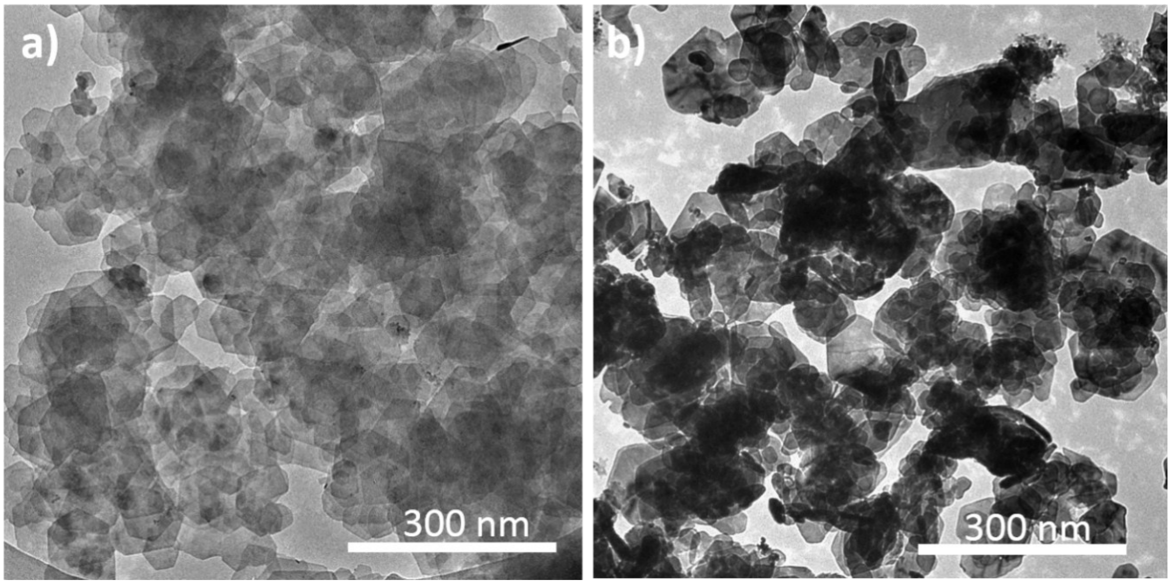

Figure S8. TEM images of the $Ni_{0.8}Fe_{0.2}$-LDH nanosheets (a) before stability test and (b) after stability test. No obvious change in morphology observed after OER catalysis.

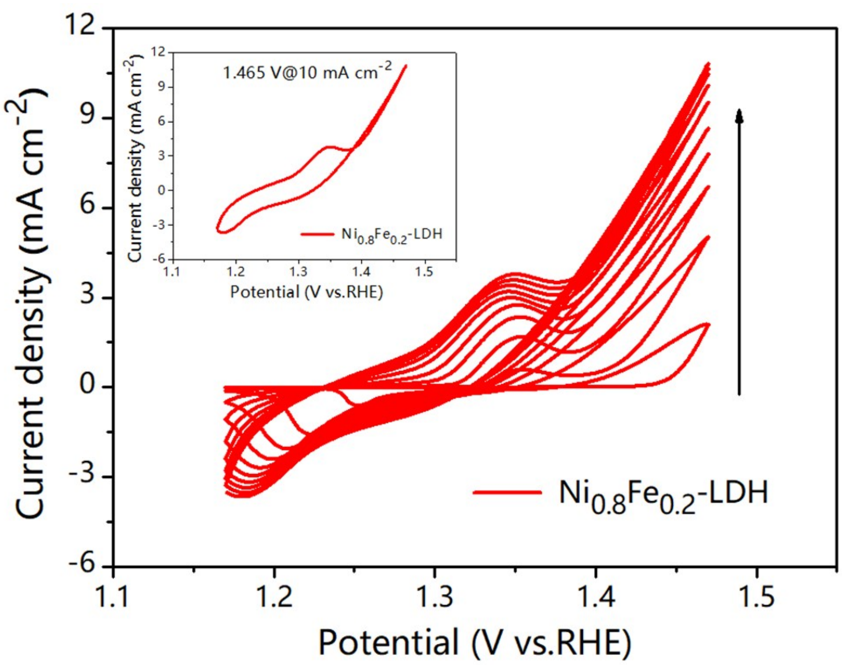

Figure S9. 20 cycles of $Ni_{0.8}Fe_{0.2}$-LDH catalyst in 1M KOH. Cycles show the obvious increasing trends of OER performance, the inset shows the current density of 20th cycle.

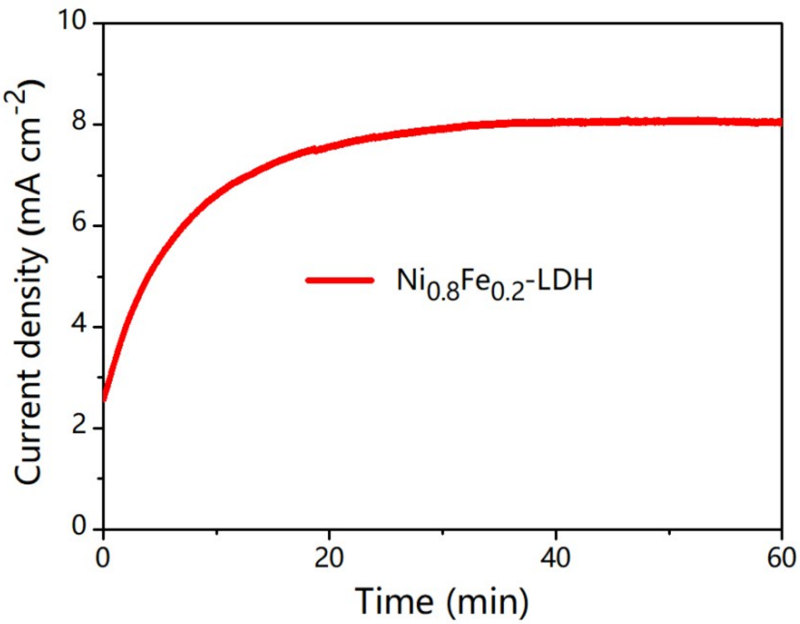

Figure S10. Time-dependent current density curve of fresh $Ni_{0.8}Fe_{0.2}$-LDH at the potential of 1.45 V *vs*. RHE.

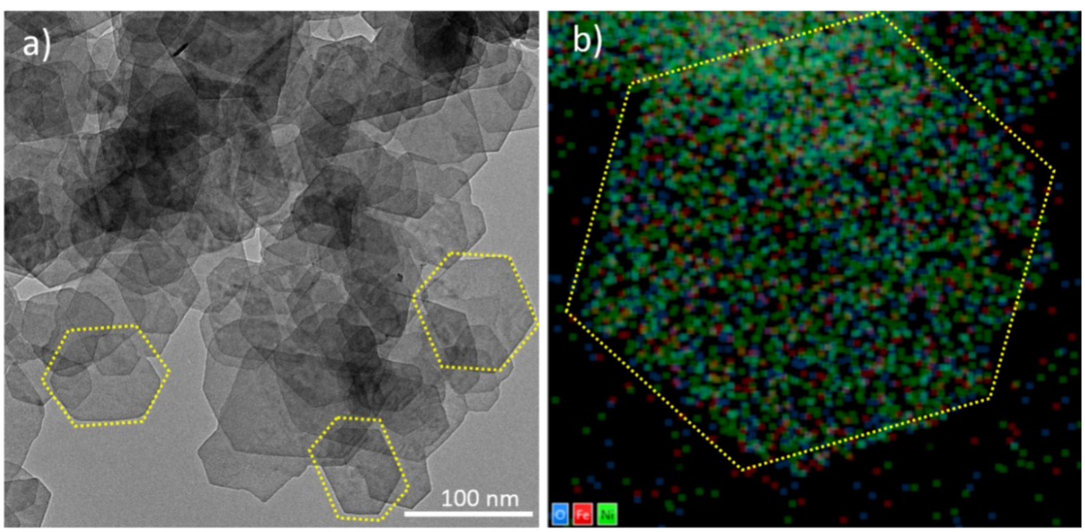

Figure S11. (a) TEM image of the $Ni_{0.8}Fe_{0.2}$-LDH nanosheets (b) HAADF-STEM image of single $Ni_{0.8}Fe_{0.2}$-LDH nanosheet with uniform distribution of elements. A high number of overall edge sites (yellow lines) of hexagonal sheets are expected to have open coordination sites that might be the active sites for OER.

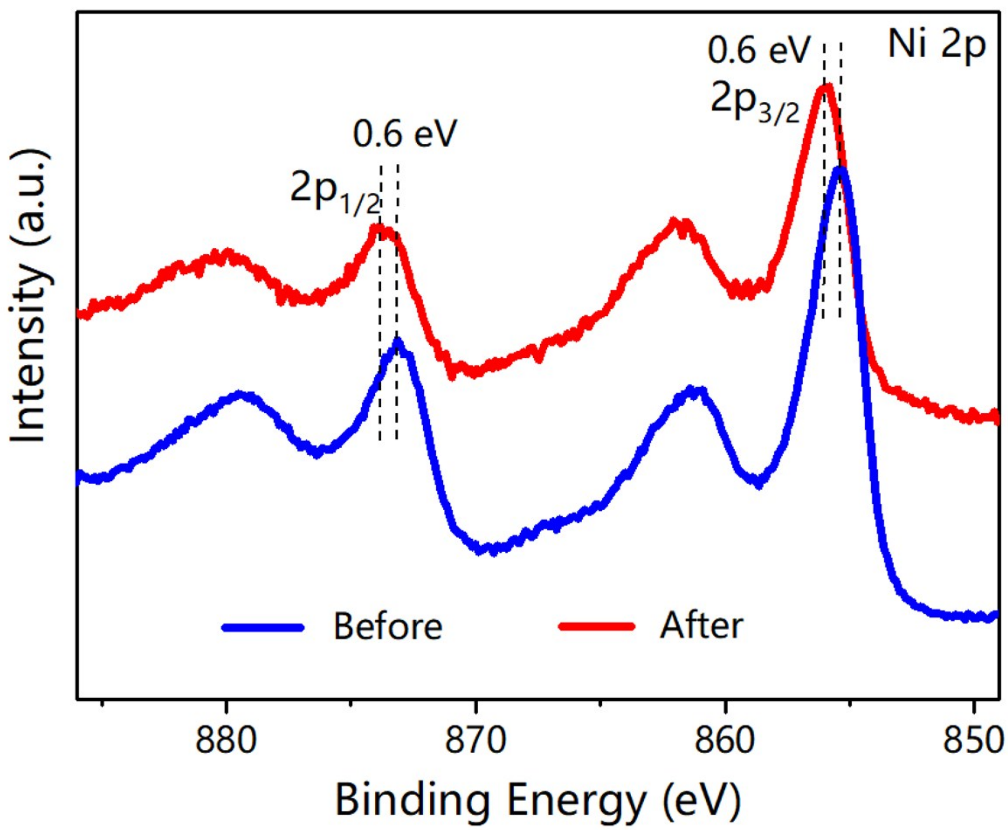

Figure S12. XPS spectra of the as-prepared $Ni_{0.8}Fe_{0.2}$-LDH nanosheets (a) before and (b) after stability test. X-ray photoelectron spectroscopy results of $Ni_{0.8}Fe_{0.2}$-LDH before and after stability test showing that, there is a positive shift of 0.6 eV for Ni(III) in $Ni_{0.8}Fe_{0.2}$-LDH after OER process. This shifting of peak implying that $Ni_{0.8}Fe_{0.2}$-LDH dynamically reform ($Ni^{2+} \rightarrow Ni^{3+}$) the active phase of the surface layer during OER.

Table S1. Fe : Ni ratios in the NiFe-LDHs samples and spinel structure determined by ICP.

Sample name	Percentage ratios of (Ni : Fe) in the final samples determined by ICP
$Ni_{0.95}Fe_{0.05}$-LDH	0.95:0.05
$Ni_{0.9}Fe_{0.1}$-LDH	0.9:0.1
$Ni_{0.8}Fe_{0.2}$-LDH	0.8:0.2
$Ni_{0.7}Fe_{0.3}$-LDH	0.7:0.3
$Ni_{0.5}Fe_{0.5}$-LDH	0.5:0.5
$NiFe_2O_4$	0.3:0.7

Table S2. OER activities of some benchmark catalysts in alkaline solution.

Catalyst	substrate	η(V)@10mA cm^{-2}	Tafel slope	References
Ni-Fe LDH hollow nanoprisms	GC	280	49.4	[2]
NiFe-LDH	GC	302	40	[3]
$Ni_{0.83}Fe_{0.17}(OH)_2$	GC	245	61	[4]
NiFe-LDH	GC	280	47.6	[5]
$Ni_{2/3}$-$Fe_{1/3}$ LDH	GC	310	76	[6]
$Fe_{(0.5)}$doped β-$Ni(OH)_2$	GC	260	32	[7]
NiFe LDH	GC	270	89	[8]
NiFe LDH	GC	240	38.9	[9]
NiFe/3D-ErGO	Au	259	33	[10]
n-NiFe LDH/NGF	GC	337	45	[11]
Ni−Fe-LDH−MoS_2	GC	250	45	[12]
NiFe-LDH	CP	322	144	[13]

NiFe-LDH	GC	263	60	[14]
$Ni_{0.8}Co_{0.1}Fe_{0.1}O_xH_y$	Ni Foam	239	45.4	[15]
NiV-LDHs	Ni Foam	257	54	[16]
$Ni_3FeAl_{0.91}$–LDH	Ni Foam	320	50	[17]
Ni_3FeN-NPs	GC	280	46	[18]
$Ni_{0.8}Fe_{0.2}$-LDH	**GC**	**235**	**41**	**This work**

References

1. L. Trotochaud, S. L. Young, J. K. Ranney and S. W. Boettcher, *J. Am. Chem. Soc.*, 2014, **136**, 6744.
2. L. Yu, J. F. Yang, B. Y. Guan, Y. Lu and X. W. D. Lou, *Angew. Chem. Int. Ed. Engl.*, 2018, **57**, 172.
3. F. Song and X. Hu, *Nat. Commun.*, 2014, **5**, 4477.
4. Q. Zhou, Y. Chen, G. Zhao, Y. Lin, Z. Yu, X. Xu, X. Wang, H. K. Liu, W. Sun and S. X. Dou, *ACS Catal.*, 2018, **8**, 5382.
5. L. Trotochaud, S. L. Young, J. K. Ranney and S. W. Boettcher, *J. Am. Chem. Soc.*, 2014, **136**, 6744.
6. W. Ma, R. Ma, C. Wang, J. Liang, X. Liu, K. Zhou and T. Sasaki, *ACS Nano*, 2015, **9**, 1977.
7. K. Zhu, H. Liu, M. Li, X. Li, J. Wang, X. Zhu and W. Yang, *J. Mater. Chem. A,* 2017, **5**, 7753.
8. Y. Jia, L. Zhang, G. Gao, H. Chen, B. Wang, J. Zhou, M. T. Soo, M. Hong, X. Yan, G. Qian, J. Zou, A. Du and X. Yao, *Adv. Mater.*, 2017, **29**, 1700017.
9. W. Zhang, Y. Wu, J. Qi, M. Chen and R. Cao, *Adv. Energy Mater.*, 2017, **7**.*1602547.*
10. X. Yu, M. Zhang, W. Yuan and G. Shi, *J. Mater. Chem. A,* 2015, **3**, 6921.
11. C. Tang, H. S. Wang, H. F. Wang, Q. Zhang, G. L. Tian, J. Q. Nie and F. Wei, *Adv. Mater.*, 2015, **27**, 4516.
12. M. S. Islam, M. Kim, X. Jin, S. M. Oh, N.-S. Lee, H. Kim and S.-J. Hwang, *ACS Energy Letter*, 2018, **3**, 952.
13. Y. Yang, L. Dang, M. J. Shearer, H. Sheng, W. Li, J. Chen, P. Xiao, Y. Zhang, R. J. Hamers and S. Jin, *Adv. Energy Mater.*, 2018, **8**, 1703189.
14. J. Zhang, J. Liu, L. Xi, Y. Yu, N. Chen, S. Sun, W. Wang, K. M. Lange and B. Zhang, *J. Am. Chem. Soc.*, 2018, **140**, 3876.
15. Q. Zhao, J. Yang, M. Liu, R. Wang, G. Zhang, H. Wang, H. Tang, C. Liu, Z. Mei, H. Chen and F. Pan, *ACS Catal.*, 2018, **8**, 5621.
16. K. N. Dinh, P. Zheng, Z. Dai, Y. Zhang, R. Dangol, Y. Zheng, B. Li, Y. Zong and Q. Yan, *Small*, 2018, **14**. *1703257.*

17. H. Liu, Y. Wang, X. Lu, Y. Hu, G. Zhu, R. Chen, L. Ma, H. Zhu, Z. Tie, J. Liu and Z. Jin, *Nano Energy*, 2017, **35**, 350.
18. X. Jia, Y. Zhao, G. Chen, L. Shang, R. Shi, X. Kang, G. I. N. Waterhouse, L.-Z. Wu, C.-H. Tung and T. Zhang, *Adv. Energy Mater.,* 2016, **6**, 1502585.